Paulo Roberto Matias Júnior

High Reliable MMC Based Electric Drive With Redundancy and Derating Strategies

Viçosa, MG

2018

Paulo Roberto Matias Júnior

High Reliable MMC Based Electric Drive With Redundancy and Derating Strategies

Monografia apresentada ao Departamento de Engenharia Elétrica do Centro de Ciências Exatas e Tecnológicas da Universidade Federal de Viçosa, para a obtenção dos créditos da disciplina ELT 490 - Monografia e Seminário e cumprimento do requisito parcial para obtenção do grau de Bacharel em Engenharia Elétrica.

Orientador: Prof. Dr. Heverton Augusto Pereira

Coorientador: Prof. M.Sc. Allan Fagner Cupertino

Viçosa, MG

2018

PAULO ROBERTO MATIAS JÚNIOR

HIGH RELIABLE MMC BASED ELECTRIC DRIVE WITH REDUNDANCY AND DERATING STRATEGIES

Monografia apresentada ao Departamento de Engenharia Elétrica do Centro de Ciências Exatas e Tecnológicas da Universidade Federal de Viçosa, para a obtenção dos créditos da disciplina ELT 490 – Monografia e Seminário e cumprimento do requisito parcial para obtenção do grau de Bacharel em Engenharia Elétrica.

Trabalho aprovado em 19 de outubro de 2018.

COMISSÃO EXAMINADORA

Heverton Augusto Pereira

Prof. Dr. Heverton Augusto Pereira – Orientador
Universidade Federal de Viçosa - UFV

Allan Fagner Cupertino

Prof. M. Sc. Allan Fagner Cupertino – Co-orientador
Centro Federal de Educação Tecnológica – CEFET-MG

Victor do Nazareth Ferreira

M. Sc. Victor de Nazareth Ferreira – Membro Externo
Universidade Federal de Minas Gerais - UFMG

William Caires Silva Amorim

Eng. William Caires Silva Amorim – Membro Externo
Centro Federal de Educação Tecnológica – CEFET-MG

VIÇOSA, MG
2018

À minha família, amigos e mestres.

Agradecimentos

Em primeiro lugar agradeço a Deus por ter possibilitado que eu chegasse até aqui e ter me dado forças para batalhar por esse sonho. Agradeço e dedico essa vitória a minha mãe, Josiene, o meu porto seguro, pelo amor incondicional, por abdicar de seus planos para que pudesse ir atrás do meu sonho e para isso não mediu esforços. Ao meu querido pai, Paulo, que mesmo não estando presente fisicamente me guardou e me fortaleceu e onde estiver sei que está imensamente contente e orgulhoso por essa conquista. A minha irmã, Thamires, pelos conselhos e por sempre estar de prontidão quando preciso. A minha namorada, Júlia, por sempre estar ao meu lado, pelas palavras de incentivo e cumplicidade. Agradeço aos amigos e familiares que andaram ao meu lado e me alegraram em momentos difíceis, me deram força e companhia para vencer cada desafio. Ao meu querido afilhado, Anthony, pela imensa alegria nos fins de semana. Agradeço também aos meus orientadores, Heverton Augusto Pereira e Allan Fagner Cupertino, pelos ensinamentos e apoio durante esses anos. A todos os outros professores do Departamento de Engenharia Elétrica, que com cada ensinamento ajudaram a me tornar um Engenheiro Eletricista. Aos queridos amigos de graduação e do GESEP, pelas marretas compartilhadas e companheirismo. Obrigado a todos que cruzaram meu caminho e me ajudaram a trilha-lo. Cada obstáculo nesses cinco anos de graduação me formaram o que sou hoje, o meu crescimento veio por cada um deles. Muito obrigado!

"Conhecimento não é aquilo que você sabe, mas o que você faz com aquilo que você sabe."
(Aldous Huxley)

Resumo

Nos últimos anos, os acionamentos elétricos de velocidade variável têm sido utilizados em diversas aplicações industriais, a fim de melhorar o desempenho dos processos e reduzir o consumo de energia. A topologia de conversores modulares multinível (CMM) tem se mostrado uma potencial solução para aplicações de média e alta tensão. Essa topologia de conversor apresenta uma estrutura inerentemente tolerante a falhas e pode ser interessante para aplicações industriais de alta confiabilidade. Baixas frequências de chaveamento em comparação com outros tipos de conversores combinadas com baixas distorções harmônicas nas grandezas de saída implicam em um cenário ideal para acionamentos elétricos de alta eficiência. Portanto, este trabalho tem como objetivo estudar o CMM para acionamentos elétricos de média tensão. A partida do motor, estratégias de redundância e uma estratégia de redução de velocidade durante falhas nas células do conversor serão avaliadas. Estas técnicas são comparadas em um estudo de caso de um motor de indução trifásico de 7,2 kV / 1,4 MW aplicado em uma bomba de polpa de minério. Serão comparadas três estratégias de redundância em termos de desempenho dinâmico e perdas e então as vantagens de cada estratégia são apresentadas.

Palavras-chaves: Conversor Modular Multinível; Acionamentos Elétricos; Estratégias de Redundância; Motor.

Abstract

In recent years, electric drives have been used in various industrial applications, in order to improve process performance and reduce energy consumption. In medium and high-voltage applications, the Modular Multilevel Converters (MMCs) have presented excellent characteristics. This converter topology features an inherently fault-tolerant structure and is a solution for high reliability industrial applications. Low switching frequencies compared to other converter types combined with low distortions in the output quantities imply an optimum scenario for high-efficiency electric drives. Therefore, this paper aims to study the MMC for medium-voltage electric drives. The motor start-up, redundancy strategies and a smart derating strategy for immediate failures are will be evaluated. These techniques are compared in a case study of a three-phase 7.2 kV/1.4 MW induction motor used as slurry pump in mining industries. The redundancy strategies are compared in terms of dynamic performance and power losses and the advantages of each strategies are presented.

Key-words: Modular Multilevel Converter; Electric Drives; Redundancy; Derating.

List of Figures

List of Tables

List of abbreviations and acronyms

MMC	Modular Multilevel Converter
HVDC	High Voltage Direct Current
STATCOM	Static Synchronous Compensator
NPC	Neutral-Point Clamped
ANPC	Active Neutral-Point Clamped
FLC	Flying-Capacitor Converter
DSCC	Double Star Chopper Cell
PR	Proportional Controller
PR	Proportional Resonant Controller
PI	Proportional Integral Controller
CMI	Common-Mode Injection
MAF	Moving Average Filter
FOC	Field Oriented Control
PS-PWM	Phase-Shifted Pulse Width Modulation
SM	Submodules
RSS	Redundant operation based on Spare Submodules
RAS	Redundant operation based on Additional Submodules
RASO	Optimized Redundant operation based on Additional Submodules
SR	Standard Redundant operation
PLECS	Piecewise Linear Electrical Circuit Simulation
IGBT	Insulated Gate Bipolar Transistor

List of symbols

C	Submodule capacitance
S_T	Bypass cwitch
N	Effective submodules per arm
M	Redundant submodules per arm
R_b	Bleeder resistor
$S1$	Lower IGBT
$S2$	Upper IGBT
$D1$	Lower diode
$D2$	Upper diode
V_{dc}	Pole to pole dc voltage
L_{arm}	Arm inductor
R_{arm}	Arm resistor
$i_{a,b,c}$	Motor phase currents (a,b,c)
$i_{u(a,b,c)}$	Upper arm currents (a,b,c)
$i_{l(a,b,c)}$	Lower arm currents (a,b,c)
v_{avg}	Submodule Average voltage submodules per phase
v^*_{avg}	Reference submodules average voltage per phase
v_{sm}	Submodule voltage
$v_{sm,f}$	Filtered submodule Voltage
v^*_{sm}	Reference submodule voltage
N_T	Operating submodules per phase
$N_{o,u}$	Operating submodules of the upper arm per phase
$N_{o,l}$	Operating submodules of the lower arm per phase

Δv_{sm}	Capacitors voltage ripple
I	Stator rms current
f	Frequency of stator voltage
i^*_{zac}	Circulating current to mitigate voltage ripple
v^*_z	Reference voltage of the circulating current control
i_{sm}	Submodule current
k_b	Proportional gain of the balancing control
ω_{ref}	Speed reference
ω^*	Speed reference after derating
ω_e	Electrical frequency
ω	Motor speed
p	Number of poles
R_s	Stator resistance
L_s	Stator inductance
L'_s	Stator transient inductance
i_d	Direct current
i_q	Quadrature current
i^*_d	Direct current reference
i^*_q	Quadrature current reference
v^*_s	Reference voltage of motor control
v^*_{com}	Common-mode voltage
v^*_u	Upper voltage reference
f_u	Utilization factor
v_{rated}	Semiconductors rated voltage
f_r	Redundancy factor
$f_{u,o}$	Utilization factor under normal conditions

$f_{u,f}$	Utilization factor after failures
k_u	Perceptual variation in the utilization factor
v_s	Stator voltage
v_d	Direct voltage
v_q	Quadrature voltage
L_r	Rotor inductance
L_m	Magnetizing inductance
λ_r	Motor flux
T	Load torque
ω_{nom}	Nominal motor speed
J	Motor moment of inertia

Contents

1 Introduction

In recent decades, the Modular Multilevel Converters (MMCs) have proven to be a great family of converters with high performance and reliability (KUMAR; PODDAR, 2018). They are mainly applied in the field of high power, such as High Voltage Direct Current transmission systems (HVDC), Static Synchronous Compensator (STATCOM) and medium-voltage adjustable speed drive systems. MMC has also been studied for energy storage and renewable energy systems (ZHANG et al., 2017; DU; LIU, 2013; JUNG; LEE; SUL, 2015; HAGIWARA; AKAGI, 2014; BIN; YONGHAI; QIAOQIAN, 2015).

The use of MMC in electric drive systems is very attractive for many factors, such as (ANTONOPOULOS et al., 2014; HAGIWARA; HASEGAWA; AKAGI, 2013; HAGIWARA; AKAGI, 2009):

- Low switching frequency, resulting in lower dv/dt and reduced damage to the motor;
- Low harmonic content, which reduces the losses and thermal stresses;
- Likely elimination of a line-frequency transformer in medium-voltage motor drive applications;
- High-quality output voltages waveforms, without the need of active filters;
- High performance, since energy costs and environmental awareness are increasing rapidly;
- High reliability and inherent fault tolerance.

The 2-level converter is the most used for low-voltage drives (PEREIRA; CUPERTINO; JUNIOR, 2017). This topology is widely used because of its robustness and simplicity when operating at this voltage level. For medium-voltage solutions up to 6.6 kV, the topologies Neutral-Point Clamped (NPC), Active Neutral-Point Clamped (ANPC) and Flying-Capacitor (FLC) become an interesting solution (KOURO et al., 2012; KAWAMURA et al., 2015). A solution for motor voltages equal or higher than 6.6 kV is based on cascade converters. The most used is provided by Robicon Corporation (HAMMOND, 1997; KAWAMURA et al., 2015). One disadvantage of this system is the need for a zig-zag transformer, which increases the losses, volume and weight of the equipment (PENG et al., 1995).

Among the MMC topologies, the most used is the Double-Star Chopper Cells (DSCC), which is widely employed in STATCOM and HVDC systems (FARIAS et al.,

2018). However, this topology has some limitations in electrical drive application during low speed and high torque. References (KUMAR; PODDAR, 2017; HAGIWARA; HASEGAWA; AKAGI, 2013; ANTONOPOULOS et al., 2014; LI et al., 2017; KUMAR; PODDAR, 2018) propose some methodologies to solve these limitations for loads whose torque is a quadratic function of the motor speed (HAGIWARA; NISHIMURA; AKAGI, 2010; LI et al., 2017). This type of load is very common in sectors such as oil and gas, pumping, food and cement industry. Some companies, such as Benshaw and Siemens, commercialize the DSCC-MMC topology for pumps, compressors and high-power blowers drive systems (AKAGI, 2017; DEKKA et al., 2017; BENSHAW, 2018; SIEMENS, 2018). Some projects and their specifications are present in Tab. 1.

Table 1 – Commercial MMC-Based Motor Drive Systems (BENSHAW, 2018; SIEMENS, 2018).

Project name	Power (MVA)	Voltage (kV)	Developed by
SINAMICS SM120	6 - 13.7	3.3 - 7.2	Siemens
M2L 3000	0.224 - 7.466	2.3 - 6.6	Benshaw

An important issue in electrical drive design is the failure capability, since failures result in high costs. The converter is the most vulnerable link, especially semiconductor devices and capacitors. However, due to advances in power electronics, many products with high reliability have been developed (SONG; WANG, 2013). The MMC is an inherent fault-tolerant topology, leading to increased system reliability when redundancy strategies are considered (AHMED et al., 2015).

Literature presents several works related to MMC redundancy. FARIAS et al. studies different techniques of redundancy applied to STATCOM, while reference (WANG et al., 2017) mentions the importance of redundancy, which allows for a maintenance scheduling, without affecting the remaining system. Reference (LIU et al., 2015) focuses on optimizing MMC redundancy control strategy. Reference (SON et al., 2012) shows the design for a HVDC system with redundant SM, targeting uninterruptible energy transfer.

Regarding the application in electrical drives, it is possible to extend the redundancy study. Instead of grid connected systems, the electric drive system does not have a minimum operating voltage. Thus, if a larger number of failures occur, the system can still operate at derating mode until maintenance can be programmed and performed. However, there is a lack of derating strategies in the literature.

1.1 Contributions

Therefore, this work proposes to fulfill this gap with a high reliable MMC based electric drive system. A 7.2 kV-1.4 MW induction motor used as slurry pump is approached. This study offers the following contributions:

- Motor start-up analysis and low-speed operation;
- Analysis of the redundancy strategies in a DSCC-MMC based medium-voltage electric drive when failures occur;
- Comparison of the redundancy strategies in terms of power losses and dynamic response;
- Smart derating strategy for continuous operation in the event of a large number of failures.

1.2 Text Organization

The work is outlined as follows. Chapter 2 proposes the MMC drive system and presents the control strategies. Also, the fault-tolerant operation with redundant SMs and derating strategy are presented in Chapter 2. Chapter 3 presents the case study and the parameters of the simulated system. Furthermore, the obtained results are shown and discussed in Chapter 4. Finally, the conclusions of this work are stated in Chapter 5.

2 Control of MMC based drive system

2.1 MMC Control and Topology

The structure of the DSCC-MMC drive system is shown in Fig. 1. As observed, this topology is also formed of a cascade association of half-bridge cells, generally consisting of two IGBTs, two diodes and a SM capacitance C. A switch S_T is usually installed in parallel with each SM. This device has the purpose of bypassing it if any fault is detected (FARIAS et al., 2018; GEMMELL et al., 2008). Thus, the topology becomes inherently fault-tolerant. Unlike the cascade converter provided by Robicon, this topology features a single dc power supply, similarly to a 2-level inverter or NPC. The MMC has N effective and M redundant SMs per arm. R_b represents the bleeder resistor.

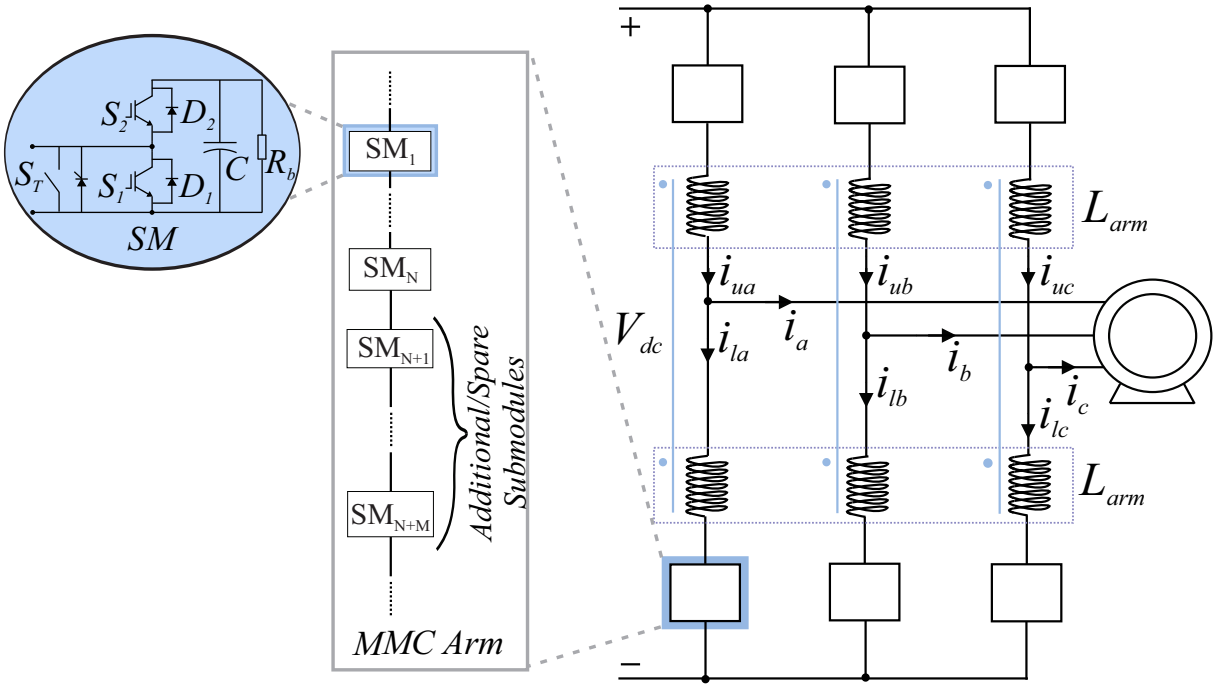

Figure 1 – Schematic of the DSCC-MMC drive system.

The arm inductors L_{arm} reduce the harmonic distortion in the circulating currents and limit short-circuit currents during faults (FARIAS et al., 2018; HARNEFORS et al., 2013). Coupled inductors are considered in this work, due to their lower volume and weight. Additionally, coupled inductors do not present equivalent inductance for output current, which is interesting for the motor control (HAGIWARA; HASEGAWA; AKAGI, 2013).

The MMC control can be divided into: averaging voltage and circulating-current control, balancing control and vector control. The proposed control strategy is presented

in Fig. 2. The block diagram for the averaging voltage and circulating current control is shown in Fig. 2 (a). The external loop controls the average voltage v_{avg} of all SMs per phase. This average voltage is computed by:

$$v_{avg} = \frac{1}{N_T} \sum_{i=1}^{N_T} v_{sm,i}, \tag{2.1}$$

where $v_{sm,i}$ is the ith SM voltage per phase. N_T is the total number of operating SMs per phase, given by:

$$N_T = N_{o,u} + N_{o,l}, \tag{2.2}$$

where $N_{o,u}$ and $N_{o,l}$ are the number of operating SMs of the upper and lower arms, respectively.

The average voltage loop leades the SMs average voltage to follow its reference v^*_{avg} and calculates the necessary circulating current to the inverter leg. This control also manages the energy exchange among the converter arms. The inner loop reduces the harmonics in the circulating current and introduces damping in the converter dynamics. The circulating current control is based on proportional resonant (PR) controller to suppress the considerable second harmonic component (XU et al., 2016).

The MMC-DSCC topology has high oscillation level in the SM capacitor voltages when the motor is operating at low frequencies. This fact is observed, since the capacitors voltage ripple is approximately inversely proportional to the stator motor frequency (HAGIWARA; NISHIMURA; AKAGI, 2010):

$$\Delta v_{sm} \approx \frac{\sqrt{2}I}{4\pi f C}, \tag{2.3}$$

where I is the stator rms current and f is the frequency of the voltage applied in the motor. Thus, large oscillations in the capacitor voltages occur during the motor start-up, which results in control instabilities and large stresses in the SM capacitors (ANTONOPOULOS et al., 2014). This work employs the ripple mitigation technique proposed by (HAGIWARA; HASEGAWA; AKAGI, 2013). This method consists of inserting a common-mode voltage and circulating current, which reduces the capacitors ripple. The common-mode waveform consists in a sinusoidal signal added to a third harmonic component. The frequency used is 54 Hz for CMI and the amplitude of the third harmonic inserted is 1/6 of the fundamental component (HAGIWARA; HASEGAWA; AKAGI, 2013).

The component i^*_{zac} presented in Fig. 2 (a) refers to the circulating current inserted to mitigate the voltage fluctuation of the capacitors at low speed. The CMI is employed at the 0 to 20 Hz range, where it has the greatest impact on the voltage ripple.

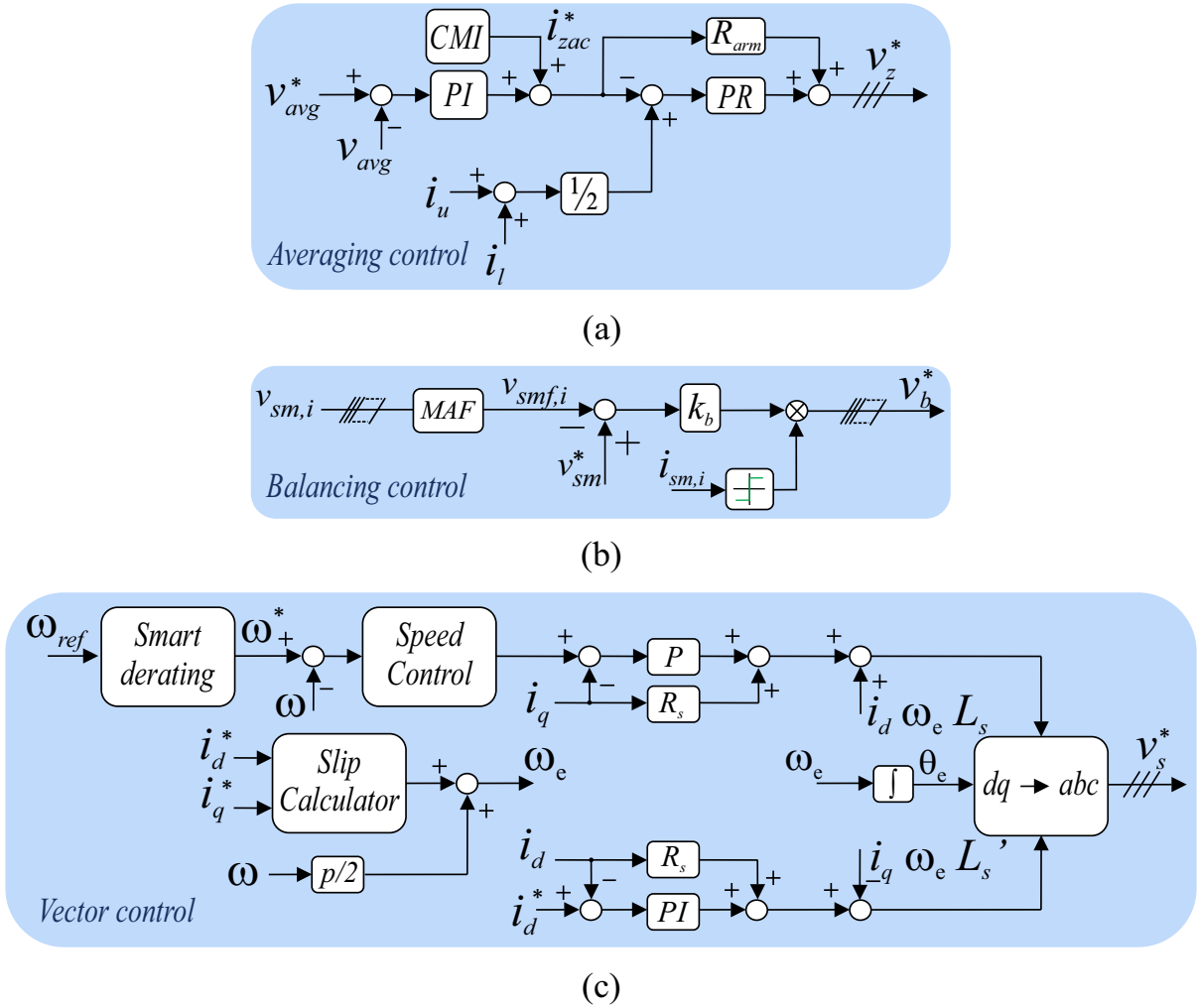

Figure 2 – Proposed control strategy for MMC Drive System: (a) Averaging and circulating-current control; (b) Balancing control; (c) Vector control.

The individual balancing control is used to ensure that the individual capacitor voltage is balanced according to the reference value (MEYNARD et al., 2002). For this strategy, the individual control is composed of a proportional controller, as shown in Fig. 2 (b). The moving average filter (MAF) attenuates the capacitor voltage ripple, which improves the individual balancing performance. Then, its output is multiplied by the arm current. The obtained signal is added to the modulator reference signal.

The last control structure is the motor speed control, as shown in Fig.2 (c). When high torque and speed performance are required, the field orientation control (FOC) is used. The control strategy used was based on (NOVOTNY; LIPO, 1996). The indirect FOC strategy was used, since the motor speed is measured to have the necessary motor flux alignment.

The modulator adds, normalizes and compares the reference signal with the carrier signals (HAGIWARA; AKAGI, 2009; HAGIWARA; NISHIMURA; AKAGI, 2010; HAGIWARA; HASEGAWA; AKAGI, 2013; SAHOO; BHATTACHARYA, 2018). A Phase-Shifted

PWM (PS-PWM) with third harmonic injection is the modulation strategy employed. The normalized reference signals per phase are given by:

$$v_u^* = v_b^* + \frac{v_z^*}{v_{sm,u}^*} - \frac{v_s^*}{v_{sm,u}^* N_{o,u}} + \frac{v_{com}^*}{v_{sm,u}^* N_{o,u}} + \frac{1}{2}\frac{N}{N_{o(u,l)}}, \tag{2.4}$$

$$v_l^* = v_b + \frac{v_z^*}{v_{sm,l}^*} + \frac{v_s^*}{v_{sm,l}^* N_{o,l}} + \frac{v_{com}^*}{v_{sm,u}^* N_{o,u}} + \frac{1}{2}\frac{N}{N_{o(u,l)}}, \tag{2.5}$$

where v_z^* is the voltage generated by the control of the circulating current, v_s^* is the reference voltage of the FOC, $v_{sm,u}^*$ and $v_{sm,l}^*$ are the SMs reference voltages of the upper and lower arm, respectively. On the other hand, v_{com}^* is the common mode voltage and $N_{o(u,l)} = min(N_{o,u}, N_{o,l})$.

2.2 MMC Fault-Tolerant Operation

2.2.1 Redundancy analysis

Due to several electrical, mechanical and environmental factors present in an industry, MMC is vulnerable to some types of failures or faults (SON et al., 2012). Nevertheless, the system should continue operating until maintenance can be programmed (KONSTANTINOU; CIOBOTARU; AGELIDIS, 2012). The MMC topology is often featured with its robustness for SM failures. Redundant SMs are inserted into each arm for fault-tolerant operation. When a fault is detected, the damaged SM should be bypassed (SON et al., 2012).

According to (FARIAS et al., 2018), the redundancy strategies can be classified as: Redundant operation based on Spare SMs (RSS), Redundant operation based on Additional SMs (RAS), Optimized Redundant operation based on Additional SMs (RASO) and Standard Redundant operation (SR).

The RSS strategy is a redundancy technique based on the concept of spare SMs (SON et al., 2012). During normal operations, the backup SM are bypassed. When a fault is detected, this faulty SM is replaced by the backup SM (LI et al., 2015). This technique has the advantage of operating with the number of SM constant and no control adaptation is employed. However, this technique affects the transient of all control variables, because the SMs inserted in the system are maintained discharged by the bleeder resistors (FARIAS et al., 2018).

The RAS strategy consists in operating the MMC with more SMs than the nominal number. When a fault occurs, the faulty SM is bypassed and the operating voltage of the SMs is maintained at the rated voltage (SAAD et al., 2015; CHOI; HAN; KIM, 2016).

Therefore, when a SM fails, the SMs voltages do not increase. Thus, small transients are observed on SM voltages.

On the other hand, RASO strategy operates the SMs with a reduced voltage under normal conditions, thus reducing the voltage stresses in the SM power devices and reduce power losses. When a fault is detected, the SMs voltages are increased to avoid overmodulation (FARIAS et al., 2018).

Finally, the SR strategy operating principle is similar to RASO. In this technique, when a failure occurs, the operating voltage of the SMs is increased (KONSTANTINOU; CIOBOTARU; AGELIDIS, 2012; AHMED et al., 2015). This is an interesting solution for applications with high numbers of SMs, without the need to use additional SMs. The utilization factor f_u can be computed by:

$$f_u = \frac{v_{sm}^*}{v_{rated}}, \tag{2.6}$$

where v_{rated} is the semiconductors rated voltage. However, to maintain a safe operation, f_u can not exceed 0.6 (FARIAS et al., 2018). Therefore, this strategy is limited by the maximum voltage stresses at the semiconductor devices and capacitors. According (FARIAS et al., 2018), for the SR strategy, the redundancy factor f_r is computed by:

$$f_r = 1 - \frac{f_{u,o}}{f_{u,f}}, \tag{2.7}$$

where $f_{u,o}$ is the utilization factor under normal conditions, and $f_{u,f}$ is the utilization factor when all admissible failures occur. In many works of literature, f_r around 10 % is employed (KONSTANTINOU; CIOBOTARU; AGELIDIS, 2012). Manipulation (2.7) and definition of the constant k_u results in:

$$k_u = \frac{f_{u,f}}{f_{u,o}} = \frac{N}{N - Nf_r}, \tag{2.8}$$

where k_u indicates the perceptual variation in the utilization factor. Since $f_{u,o} = 0.5$ is widely used, $k_u = 0.6/0.5 = 1.2$ would be the limit. However, once the SMs voltages present ripple, a safety margin is adopted. Thus, $k_u = 1.15$ is employed. Fig. 3 shows the effect of the number of SMs in the k_u ratio for $f_r = 0.1$. As observed, applications with lower number of SMs exceed the range of $k_u = 1.15$. Once MMC based drive systems typically employ few SMs, the SR strategy is not suitable because it results in large voltage stress in the SMs.

Regarding the implementation, the reference values for the average voltage control v_{avg}^* and the balancing control v_{sm}^*, depend on the redundancy strategy used. For the RSS

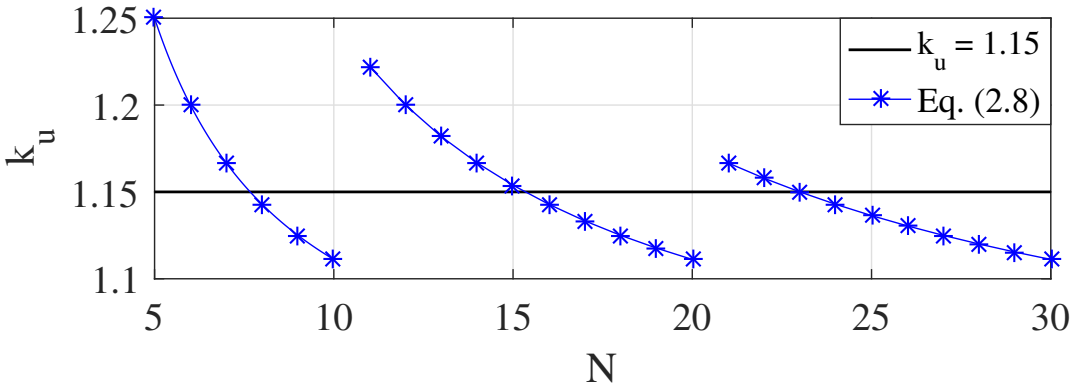

Figure 3 – Redundancy limit for SR for some number of SMs.

and RAS strategies, the voltage reference for the individual control is calculated by:

$$v_{sm}^{*} = \frac{V_{dc}^{*}}{N}, \tag{2.9}$$

where V_{dc} is the nominal pole-to-pole voltage. Even during faults, the average voltage references do not change in RSS and RAS strategies. Therefore, the average reference voltage per phase is calculated by:

$$v_{avg}^{*} = \frac{V_{dc}^{*}}{N}. \tag{2.10}$$

However, in the RASO strategy, when a fault is detected, the reference SMs voltages is increased. Thus, the reference voltage for all SMs and the average reference voltage for RASO strategies are computed by:

$$v_{sm}^{*} = \frac{V_{dc}^{*}}{N_{o,u,l}}, \tag{2.11}$$

$$v_{avg}^{*} = \frac{V_{dc}^{*}}{N_{o,u,l}}. \tag{2.12}$$

2.2.2 Derating strategy

As previously mentioned, industrial equipment is susceptible to several factors that can lead to failures. When all redundant SMs have been used, failures can still occur. Under such conditions, a smart derating strategy is proposed in this paper. When the number of failures exceeds the designed redundancy factor, the voltage applied to the motor is reduced.

Fig. 4 illustrates this problem. When a fault occurs in a MMC based electric drive without redundant SM, the insertion index is increased, since the MMC will have less SMs to synthesize the motor voltage. To circumvent this increase in the insertion index

and avoid overmodulation, the smart derating strategy is used to keep the insertion index constant when more failures occur. Thus, the motor power is reduced by motor speed reduction. This is possible due to the quadratic characteristic of the load.

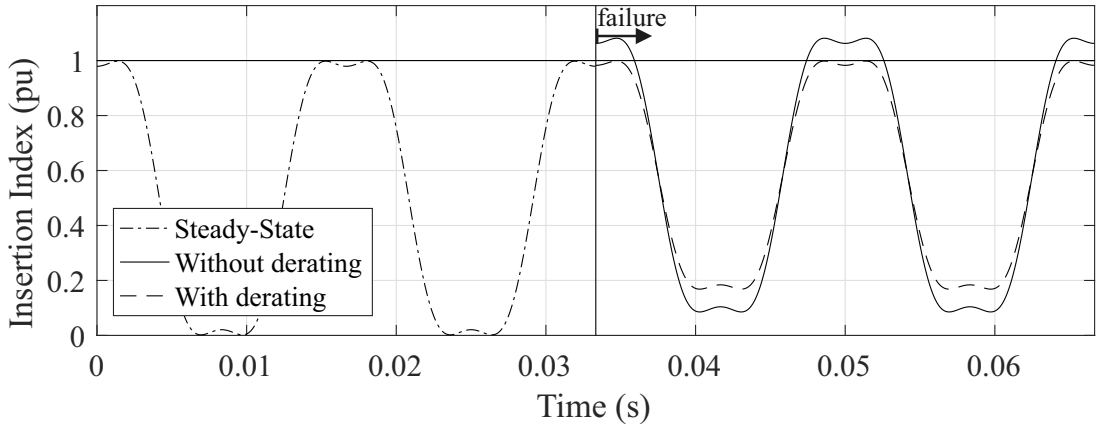

Figure 4 – Effect of smart derating on the insertion index.

The voltage of the stator machine in d-q can be represented by (NOVOTNY; LIPO, 1996):

$$v_s = \sqrt{v_d^2 + v_q^2}, \tag{2.13}$$

where, v_d and v_q are the direct and quadrature voltages, respectively.

On the other hand, the steady-state voltages can be described by (NOVOTNY; LIPO, 1996):

$$V_d = R_s I_d - \omega_e L'_s I_q, \tag{2.14}$$

$$V_q = R_s I_q + \omega_e L_s I_d, \tag{2.15}$$

where R_s is the stator resistance, I_d and I_q are the steady-state currents of the direct and quadrature axis, respectively. ω_e is the angular electric frequency of the voltage applied in the motor, L'_s is the stator transient inductance, L_s is the stator self inductance. The current I_q can be written according to the torque as:

$$I_q = \frac{4L_r}{3pL_m\lambda_r}T, \tag{2.16}$$

where L_r is the rotor self inductance, p is the number of poles, L_m is the magnetizing inductance and λ_r is the motor flux. On the other hand, the load torque is given by:

$$T = k\omega_m^2, \tag{2.17}$$

where the constant k is calculated to have the rated torque T_{nom} at nominal speed ω_{nom}. Using relations (2.14) and (2.15) and $\omega_e \approx \omega_m$, the equation (2.13) can be written as:

$$v_s = \sqrt{a\omega_m^6 + b\omega_m^4 - c\omega_m^3 + d\omega_m^2 + e^2}, \tag{2.18}$$

where the constants a, b, c, d and e are respectively:

$$a = \left(\frac{2R_s L_r L_s k}{3pL_m^2}\right)^2 + \left(\frac{L_r L'_s k}{3pL_m^2 I_d}\right)^2, \tag{2.19}$$

$$b = \left(\frac{R_s L_r k}{3pL_m^2 I_d}\right)^2, \tag{2.20}$$

$$c = \left(\frac{2R_s L_r L'_s k}{3pL_m^2}\right)^2, \tag{2.21}$$

$$d = (L_s I_d)^2, \tag{2.22}$$

$$e = (R_s I_d)^2. \tag{2.23}$$

For high speed operation, most of the voltage synthesized by the MMC is due to the FOC and the average control, since the voltage generated by the circulating current and balancing controls are very low at high speeds. Therefore, the normalized voltages synthesized for the upper and lower arm can be approximated by:

$$v_u \approx -\frac{v_s}{v^*_{sm,u} N_{o,u}} + \frac{1}{2}\frac{N}{N_{o,u,l}}, \tag{2.24}$$

$$v_l \approx \frac{v_s}{v^*_{sm,l} N_{o,l}} + \frac{1}{2}\frac{N}{N_{o,u,l}}. \tag{2.25}$$

Thereby, the maximum value of the synthesized upper and lower arm normalized voltages are given by:

$$max(v_{u,l}) = max\left(\frac{v_s}{v^*_{sm,l} N_{o,u,l}}\right) + max\left(\frac{1}{2}\frac{N}{N_{o,u,l}}\right) \leq 1. \tag{2.26}$$

By assuming a modulation index equal to 1 to avoid overmodulation, the following result is obtained:

$$v_s + v^*_{sm} N_{o,u,l}\left(\frac{1}{2}\frac{N}{N_{o,u,l}} - 1\right) = 0. \tag{2.27}$$

Thus, replacing (2.18) in (2.27) and solving for ω_m, the necessary reduction of the speed can be obtained according to the number of failures.

2.3 Thermal Model

The junction temperature T_j and case temperature T_c of the semiconductor devices are important variables that directly affect the power losses and lifetime. The methodology employed is based on a look-up table of losses obtained from the power modules datasheets. The thermal model employed is presented in Fig. 5 (TU; XU, 2011).

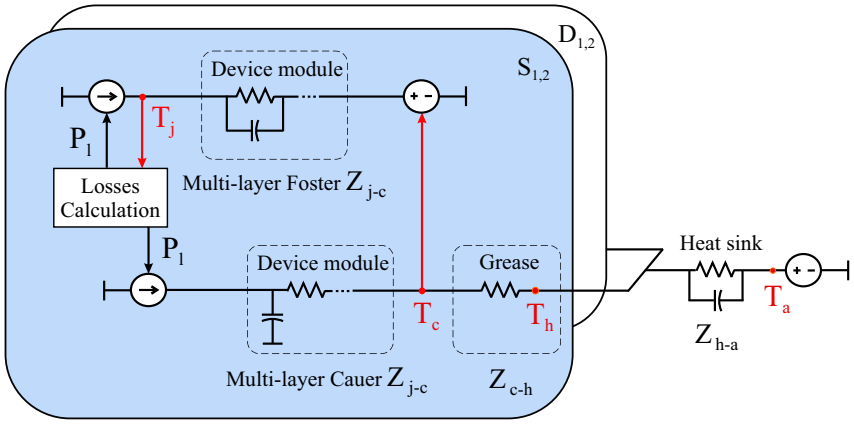

Figure 5 – Thermal model of the power devices in the half-bridge SM with a common heatsink.

Generally, the junction-to-case thermal impedance Z_{j-c} and the case-to-heatsink thermal impedance Z_{c-h} are obtained from the datasheets. The heatsink-to-ambient thermal impedance Z_{h-a} presents a larger capacitance when compared to power module which is generally disregarded in thermal simulations. Additionally, the thermal resistance can be approximated by (FARIAS et al., 2017):

$$R_{h-a} = 6N\frac{T_{h,max} - T_a}{P_{lt}}, \tag{2.28}$$

where P_{lt}, $T_{h,max}$ and T_a are the total power losses of the converter, maximum heatsink temperature and ambient temperature, respectively. Considering $T_a = 40\,^{\circ}\text{C}$, $T_{h,max} = 80\,^{\circ}\text{C}$ and P_{lt} as 0.5% of rated power in the worst case, $R_{h-a} = 0.168K/W$ is obtained.

3 Case Study

In this work, it was considered the electric drive of a high power induction motor developed by WEG, Fig. 6, used as slurry pump in mining industries (WEG, 2018a). The motor was considered star-connected and the plate data are presented in Tab. 2.

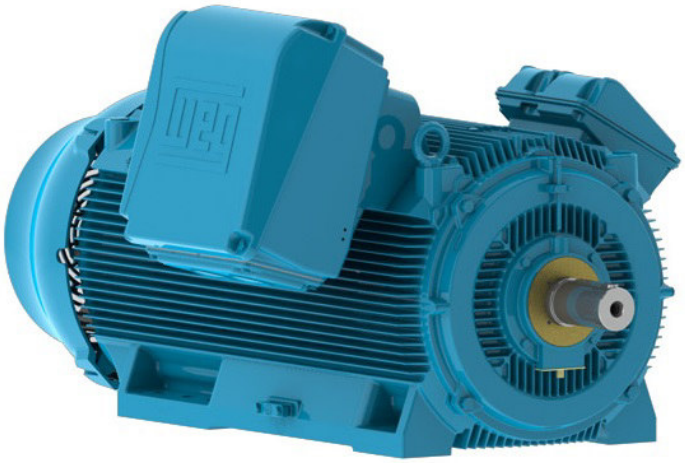

Figure 6 – WEG HGF motor (WEG, 2018b).

Table 2 – Plate data of the induction motor.

Parameter	Value
Rated active power (P)	1.4 MW
Rated rms line-to-line voltage (v_m)	4.16/7.2 kV
Rated frequency (f)	60 Hz
Rated rotational speed (n_m)	1792 rpm
Rated power factor	0.87
Rated efficiency (η)	96.7 %
Number of poles (p)	4
Rated torque (T_{nom})	7.46 kN.m
I_p/I_{nom} ratio	7.2
T_{max}/T_{nom} ratio	2.6
Motor moment of inertia (J)	29.43 kg.m^2

Due to the difficulty of finding the motor parameters in this power range, the iterative methodology proposed by (PEDRA; CORCOLES, 2004) is used in this work. Thus, it is possible to estimate electrical parameters of the induction motor equivalent circuit that guarantee the minimum error of the motor plate data. The parameters obtained are presented in Tab. 3. In this turn, the MMC ratings are shown in Tab. 4.

The load is modeled by a quadratic torque curve, emulating the behavior of a high power slurry pump. The load proportionality constant (k) is calculated to have the

Table 3 – Electrical parameters of the induction motor.

Parameter	Value
Rotor resistance (R_r)	0.15386 Ω
Stator resistance (R_s)	0.13735 Ω
Magnetizing inductance (L_m)	217.3 mH
Stator leakage inductance (L_{ls})	7.34 mH
Rotor leakage inductance (L_{lr})	7.34 mH

Table 4 – MMC parameters.

Parameter	Value
Rated apparent power (S)	2 MVA
Pole to pole dc voltage (V_{dc})	12 kV
Arm inductance (L_{arm})	7.7 mH
Arm resistance (R_{arm})	0.065 Ω
SM capacitance (C)	2 mF
Nominal SM voltage ($v_{sm,n}$)	1.71 kV
Switching frequency (f_s)	945 Hz
Number of SMs (N)	7 per arm
Number of additional/spare SMs (M)	1 per arm

nominal torque at rated speed. As the case studied is an industrial pump system, the inertia of the load can be approximated by the moment of inertia of the motor.

The failure scenario used in this work consists of an asymmetrical failure. When some SM of one arm fail, the other arms continue operating normally. Three failures are considered in the operation of the system. First one, the motor is operating in steady-state with nominal power and with redundant SM available. When the fault is simulated the redundancy strategies will act in order that the system can continue operating in the nominal condition. In the second fault, the motor is in nominal condition, but it does not have redundant SM, since they were used in the first fault. In this case, the first derating strategy are applied, reducing the motor speed when the second fault occurred. Then, it is considered the third fault when the motor reaches in steady-state with the reduced speed. At this stage the motor speed is reduced again, thus, the motor can operate with 5/7 of the SMs.

Simulations are performed in PLECS environment. A ABB IGBT part number 5SNG 0250P330305 of 3.3 kV-250 A is selected for this application (ABB SWITZERLAND LTD., 2014). Fig. 7 shows the MMC based electric drive system rated at 7.2 kV and 1.4 MW.

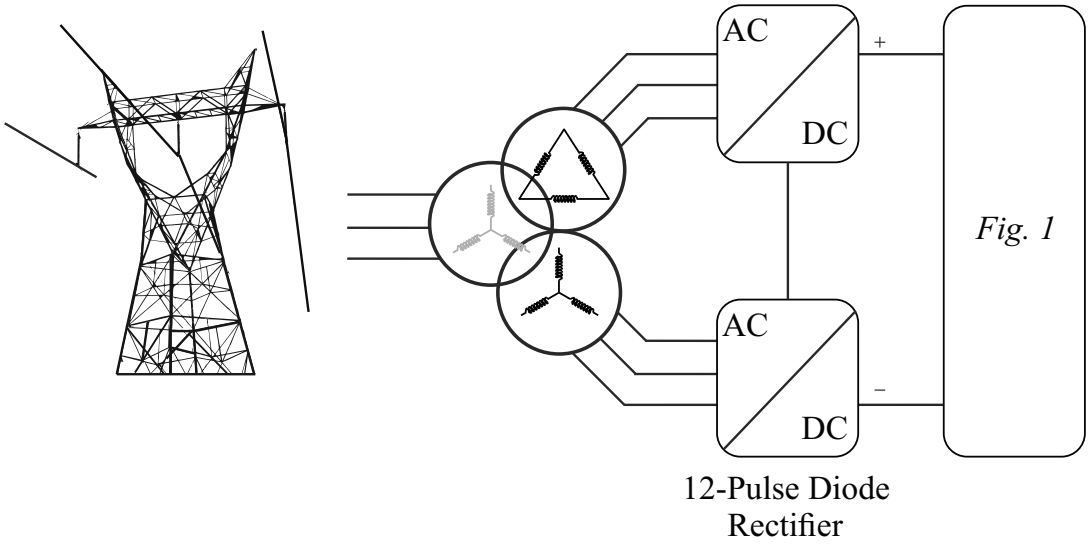

Figure 7 – 7.2 kV 1.4 MW MMC based electric drive system .

4 Results and Discussion

4.1 Start-up dynamic performance

Fig. 8 shows the torque and speed profile applied to the system. Fig. 8 (a) shows the applied torque characteristic and the electromagnetic torque. The error in the transient is due to the acceleration of the motor, where the developed torque must be higher than the load torque. The oscillations present at $t = 5.3$ s are due to the end of the CMI. There is a very low ripple in the torque in steady-state, less than 0.5 %, which tends to minimize vibrations in the motor, since the converter has 7 SMs and, consequently, 15 levels of phase voltage. The speed profile adopted in this work can be observed in Fig. 8 (b). The motor is accelerated from 2 to 12 seconds, and, in steady-state, the motor speed is maintained at 1800 rpm. In addition, this figure illustrates the speed error during the start-up, which results in a maximum error of 1.5 rpm in $t = 2$ s. The small speed variation in $t = 5.3$ s are also due to the end of the CMI used.

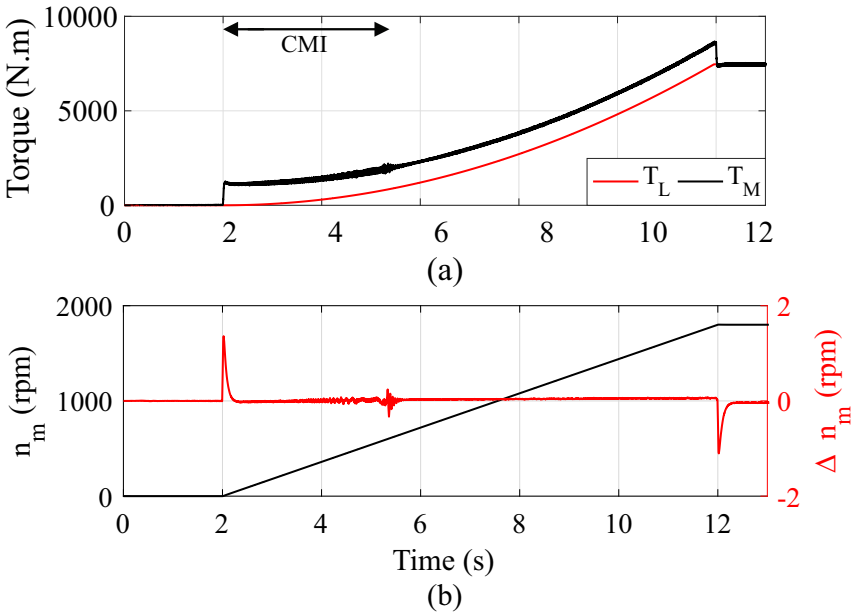

Figure 8 – Start-up of the MMC based electric drive: (a) Torque; (b) Mechanical speed and speed error.

Fig. 9 shows the converter dynamics. Initially, all capacitors of the SMs were considered charged. At 0.1 seconds the direct axis current is inserted in order to magnetize the motor. This behavior can be analyzed in the motor currents, shown in Fig. 9 (a), when the dc component is applied in the machine. After 2 seconds, a speed ramp is applied to accelerate the motor. At this time, the CMI strategy is inserted in order to mitigate ripple under lower frequency of the capacitor voltages. In addition, the same figure shows

a quadratic increase in the currents amplitude, which is also presented in Fig. 9 (b). When the motor reaches 1800 rpm, a small drop in motor and arm currents are observed.

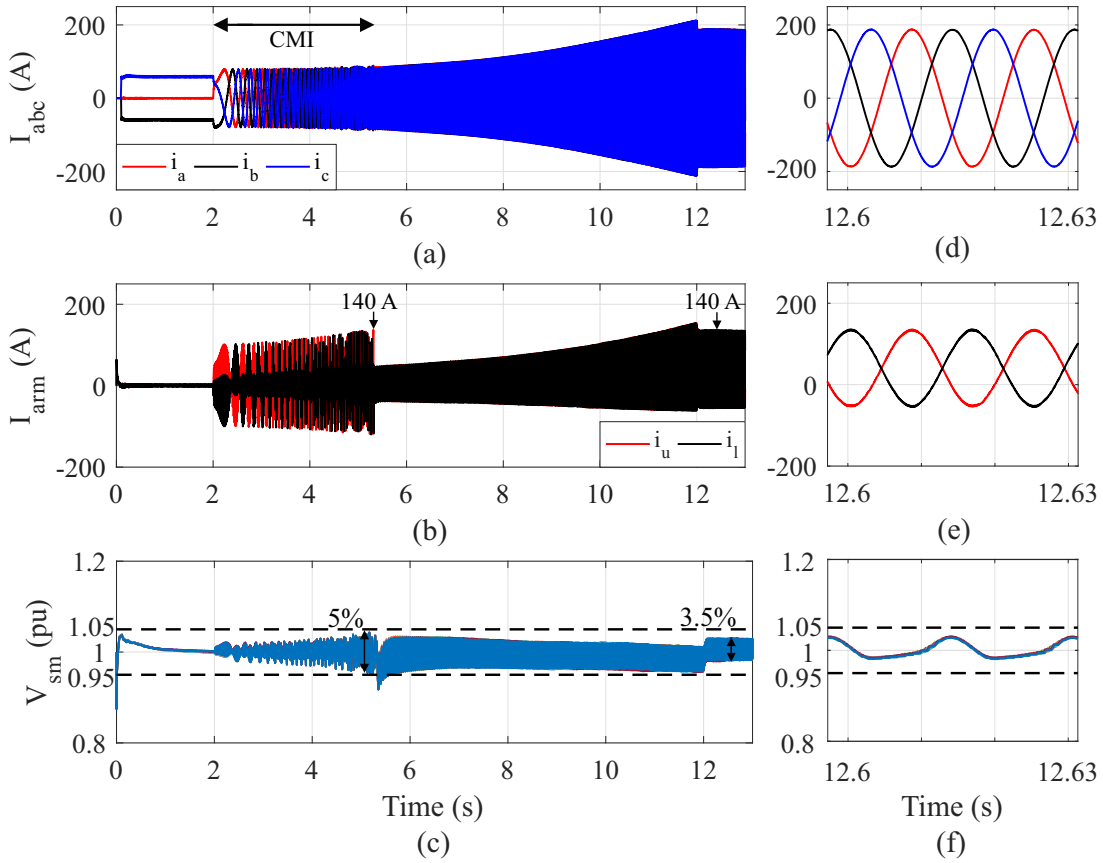

Figure 9 – Effect of the startup in the dynamics of the MMC: (a) Motor currents; (b) Arm currents; (c) SM voltages; (d) Detail for motor currents; (e) Detail for arm currents; (f) Detail for SM voltages.

Moreover, Fig. 9 (b) illustrates the insertion of the i^*_{zac}. This component is injected into the system until $t = 5.3$ s, when the frequency applied to the motor is lower than 20 Hz. It is also demonstrated that the peak of the current inserted in low frequency is similar to the arm currents in steady-state. The SMs capacitor voltages of the upper arm for the a-phase are shown in Fig. 9 (c). As observed, the capacitor voltages in the steady-state have a ripple of 3.5 %, that is, within the limit of 5 % dashed band. During the transient, the ripple reaches a maximum of 5 %, which indicates that the CMI strategy and choice of capacitance are well adjusted.

4.1.1 Dynamic Performance of Redundancy Strategies

The simulation considers a failure of one SM at 14 seconds. The capacitor voltages in pu of the upper arm for the a-phase are illustrated in Fig. 10. As observed in Fig. 10 (a), the SM voltages are balanced for the RAS strategy, since the reference voltage of the SMs is maintained constant in this strategy. Therefore, this strategy has a lower transient

on the capacitor dynamics when a fault occurs. Additionally, the maximum value of SM voltages in steady-state does not exceed 5 %, thus validating the redundancy strategy.

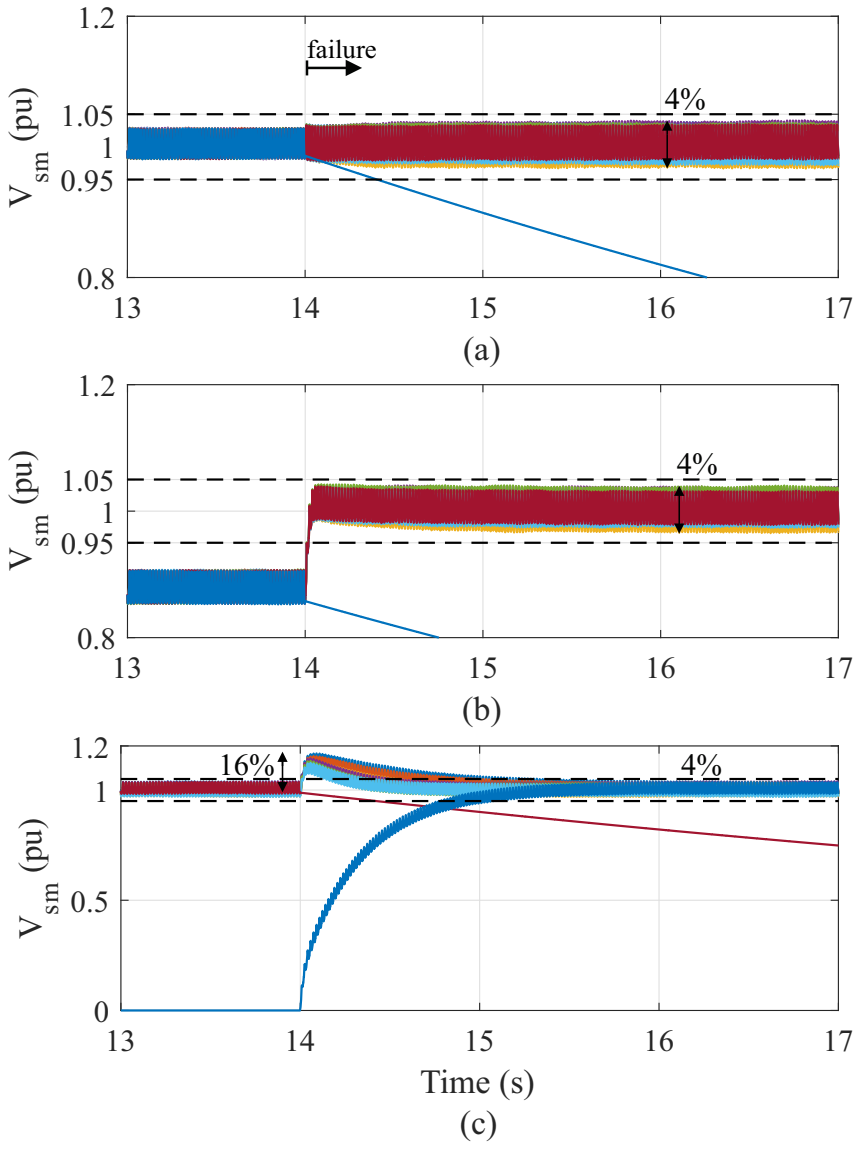

Figure 10 – Effect of the redundancy strategies on the dynamics of the SM voltages: (a) RAS; (b) RASO; (c) RSS.

For the RASO strategy, as illustrated in Fig. 10 (b), the SMs operate with reduced voltage under normal conditions, that is 0.9 pu. When failures occur, the SM voltages are increased in order to avoid overmodulation. The increased reference voltage generates a transient response at the capacitor voltages, which reach the steady-state rapidly, maintaining the voltage at 1 pu. As observed, the capacitor voltages do not exceed the tolerance range of 5 %.

Fig. 10 (c) illustrates the SMs voltage for the RSS strategy. When the failure occurs, the spare SMs are inserted and their charging process is started due the MMC control. During the charging process, the SM voltages reach 1.16 pu. After 2 s, the spare

SM charging process is finished and the converter reaches steady-state. It is important to observe that the number of SMs does not change in the RSS strategy, since the faulty and spare SMs are exchanged. Although a significant transient is observed during the charge of the spare SM, the voltages have a ripple of less than 5 % in a steady-state.

The impact of the redundancy strategies on the arm currents for the phase-a can be analyzed in Fig. 11.

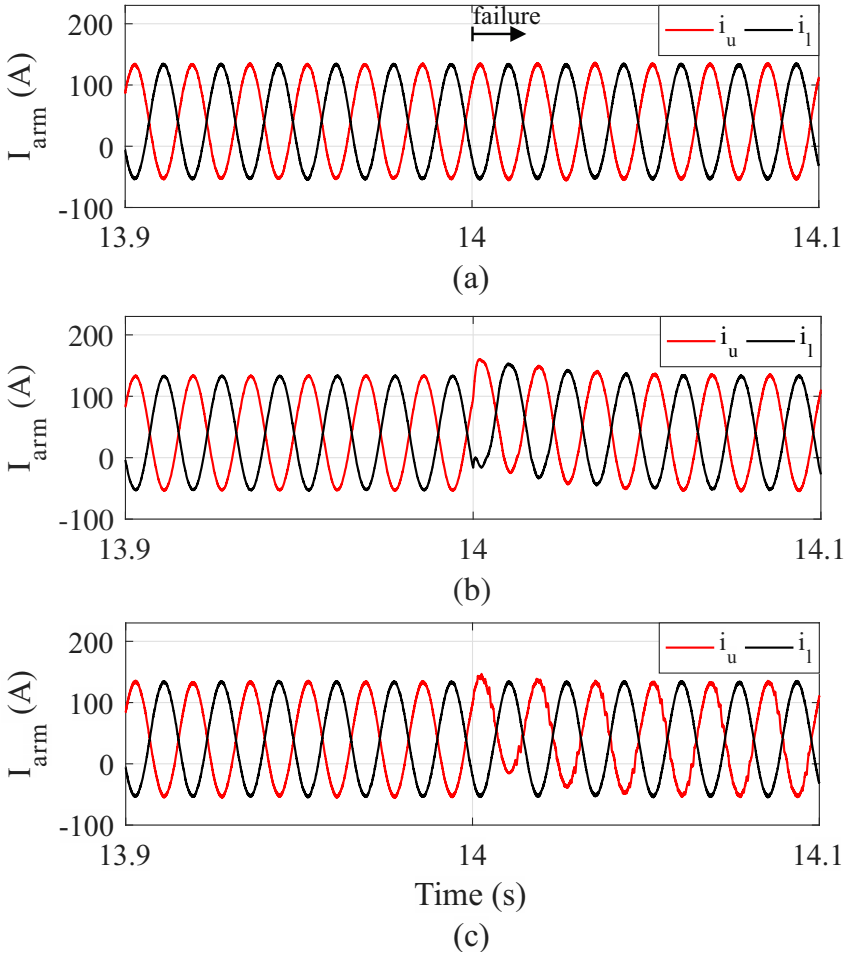

Figure 11 – Effect of the redundancy strategies on the dynamics of the arm currents of the MMC: (a) RAS; (b) RASO; (c) RSS.

As observed in Fig. 11 (a), no significant transients is observed for the RAS strategy. RASO presents an overshoot of 15 % when failure occurs, due to the increased voltage reference, as observed in Fig. 11 (b). Finally, Fig. 11 (c) presents the response for RSS. As observed, this strategy presented an overshoot of 8 % and a distortion in the arm currents. These distortions are consequences of charging spare SMs, where the individual control imposes a greater proportional action to carry out the charging process.

Fig. 12 shows the electrical and mechanical performance of motor control. The electromagnetic torque and the speed error for all redundancy strategies are presented in Fig. 12 (a) and Fig. 12 (b), respectively. As observed, when a fault occurs, the RASO

strategy presents greater error during the transient, however the speed error is only 0.28 rpm, without significantly impacting the FOC control.

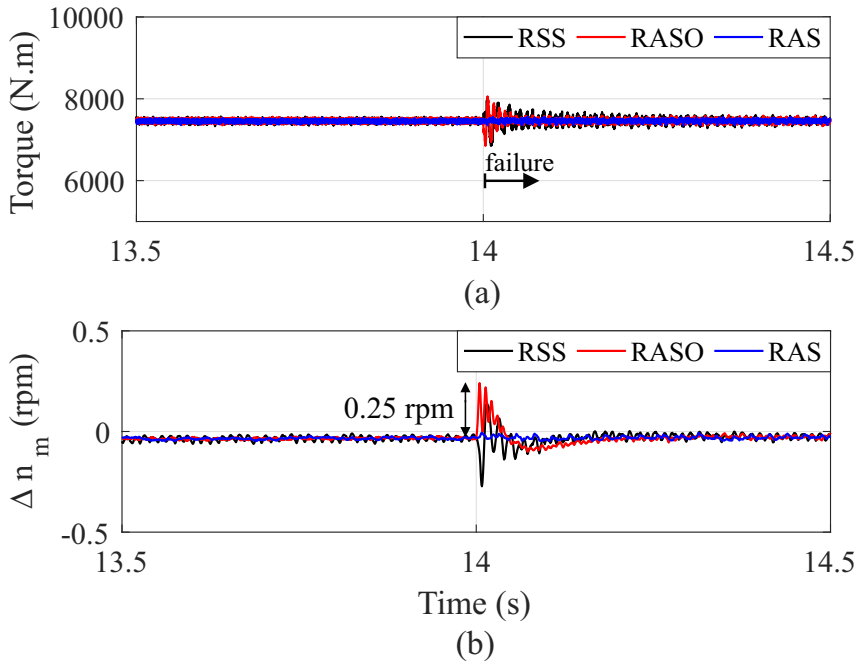

Figure 12 – Effect of the redundancy strategies in the dynamic of motor: (a) Torque; (b) Speed error.

Finally, the semiconductors devices power losses were obtained in steady-state before the failure. The obtained values are represented in Tab. 5. As observed, the RAS strategy has greater losses, since it works with additional SM. The RASO strategy has slightly lower losses, due to the fact that the semiconductor devices work with reduced voltage before the failure. In turn, the RSS strategy does not affect the efficiency of the system, since the MMC operates with the nominal number of SM, once the spare SMs are bypassed.

Table 5 – Semiconductors devices power losses before the failure.

Strategy	Conduction (W)	Switching (W)	Increase of losses
RAS	5030	8530	14.72 %
RASO	4950	7380	4.31 %
RSS	4380	7440	0 %

4.1.2 Dynamic Performance of Smart Derating

Fig. 13 presents the solution of (2.27) using the parameters of Tab. 2 and 4. Note that despite the nonlinear characteristic of (2.27), the speed reduction is approximately a line with an angular coefficient $\alpha = -2$. This is due to two facts: firstly, since the motor is controlled by the FOC, the motor operation at high speeds is similar to a ratio V/f

constant. This would imply a proportional reduction. Moreover, as failures occur, the difference between the dc link and the sum of the capacitor voltages increases and an additional voltage portion must be used to limit the circulating current. This portion is represented by the term $\frac{1}{2}\frac{N}{N_{o,u,l}}$, which leads to a reduced voltage to avoid overmodulation.

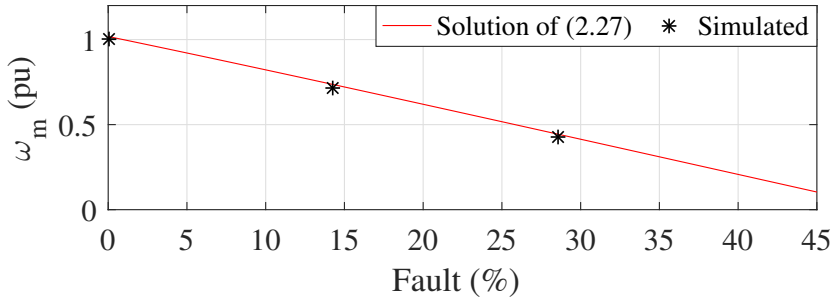

Figure 13 – Speed reduction according to the percentage of SM fault.

Finally, the smart derating strategy implemented is analyzed. Fig. 14 shows the speed profile for maintaining the MMC operating correctly. The first derating occurs in t = 17 s, where the faulty SM is bypassed. As already discussed, the speed should be reduced to 28 % to maintain the modulation index constant. After reaching the final condition at t = 19 s, the motor speed is kept constant. Next, another SM is bypassed in the system at t = 20 s. The speed is then reduced to 46 % of the rated speed, and reaching the final value in 22 seconds.

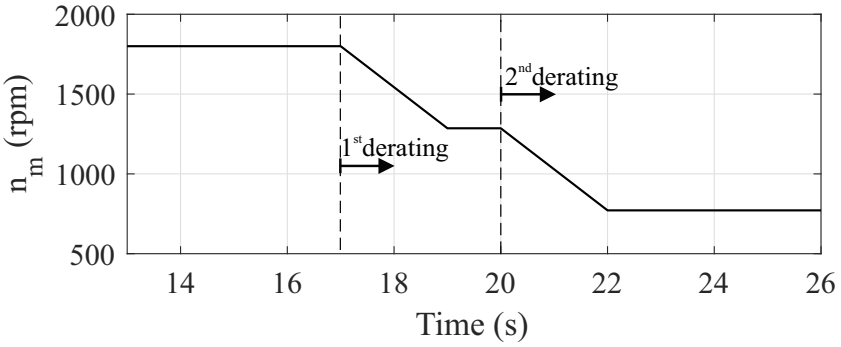

Figure 14 – Reduction of reference speed computed by the smart derating.

The dynamics of the MMC and the motor during the smart derating strategy are shown in Fig. 15. Fig. 15 (a) shows the dynamic behavior of the upper arm capacitor voltages from phase-a. It is observed an overshoot of 1.08 pu at t = 17 s due to SM failure. In steady-state, at t = 19 s, the capacitor voltage is already within the 5 % ripple range. In the third fault, at t = 20 s, the overshoot is higher, with a peak of 1.105 pu. This can be explained by the low number of SMs operating. However, the ripple in steady-state is 7 %, thus which allows to maintain a good functioning.

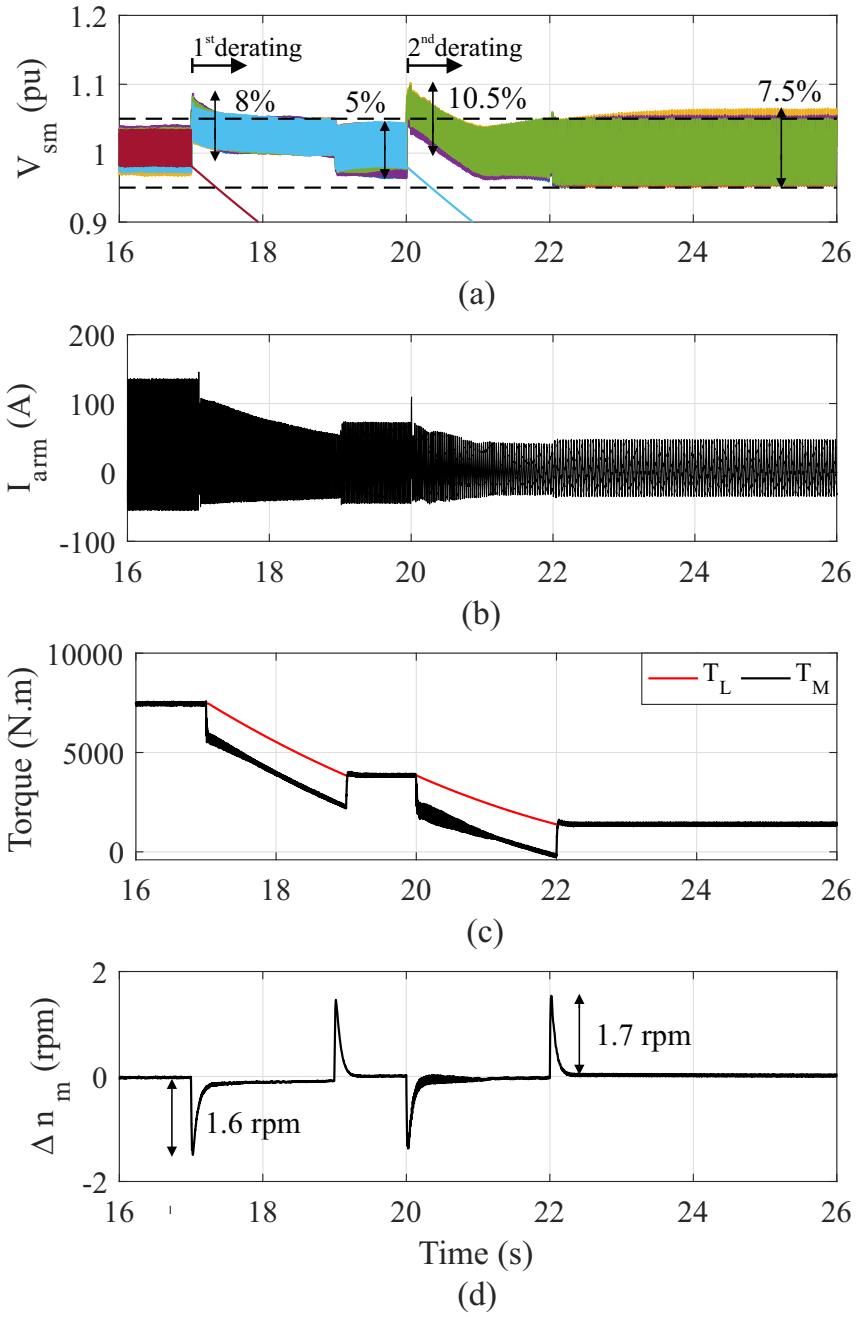

Figure 15 – Smart derating strategy: (a) SM voltages; (b) Upper arm currents; (c) Torque; (d) Speed error.

The upper arm current of phase-a is shown in Fig. 15 (b). During the second failure, at $t = 17$ s, a small overshoot is observed for a short period of time. While the speed is being reduced, from 17 to 19 seconds, it is possible to analyze the current reduction, due to the load characteristic. For the third fault, a smaller current peak is observed, almost reaching 115 A.

The motor dynamics due to the smart derating strategy can be analyzed in Fig. 15 (c) and (d). The torque applied to the motor, and the developed torque on the shaft are shown in Fig. 15 (c). This figure also shows the reduction of torque due to the speed

reduction strategy used. In addiction, the speed error is shown in Fig. 15 (d). Despite the considerable transients present during the derating strategy, the speed error is very low. In the first derating strategy, the highest speed error was 1.6 rpm, and in the second, it was 1.75 rpm. Therefore, it can be concluded that the smart derating strategy proposed in this work presented good dynamic results both in the MMC and in the motor.

5 Conclusion

This work presented strategies to explore the redundancy capability of the MMC drive system. Three redundancy strategies were used and their performances were obtained through a case study of an electric drive of a 1.4 MW slurry pump. In addition, a CMI strategy was used to mitigate the high ripple when the motor operates at low speeds and allow the drive to operate properly under such conditions.

The comparison presented is supported by simulation results. The RAS strategy has a better dynamic behavior, since its voltage reference is maintained fixed. In turn, the RSS strategy has greater impact on the dynamics due to the capacitor charging process. However, one advantage is that only N SMs are operating, which does not require the control to be adaptive. Finally, the RASO strategy advantage is allowing semiconductors and capacitors to operate at lower voltages, which reduces the stresses of these components. The SR strategy is not suitable because it results in large voltage stresses in the SMs.

A new smart derating strategy has been proposed, thus, the MMC can continue to operate when a large number of failures occur. Therefore, pump speed is reduced through the methodology developed in this work. The derating proposed in this work was verified through the dynamic behavior of the MMC and the motor.

References

ABB SWITZERLAND LTD. *HiPak IGBT Module - 5SNG 0250P330305*. [S.l.], 2014. Doc. No. 5SYA 1426-02. Disponível em: <https://library.e.abb.com/public/5d0d114ffb242b83c1257a55002ba492/5SNG%200250P330305%205SYA%201426-02%2001-2014.pdf>. 28

AHMED, N. et al. Performance of the modular multilevel converter with redundant submodules. In: *IECON 2015 - 41st Annual Conference of the IEEE Industrial Electronics Society*. [S.l.: s.n.], 2015. p. 003922–003927. 16, 22

AKAGI, H. Multilevel converters: Fundamental circuits and systems. *Proceedings of the IEEE*, v. 105, n. 11, p. 2048–2065, Nov 2017. ISSN 0018-9219. 16

ANTONOPOULOS, A. et al. Modular multilevel converter ac motor drives with constant torque from zero to nominal speed. *IEEE Trans. on Industry Applications*, v. 50, n. 3, p. 1982–1993, May 2014. ISSN 0093-9994. 15, 16, 19

BENSHAW. *M2l 3000 Series Medium Voltage Motor Drive.* [S.l.], 2018. Disponível em: <http://www.benshaw.com/uploadedFiles/Literature/Benshaw%20M2L%20Brochure.pdf>. 9, 16

BIN, R.; YONGHAI, X.; QIAOQIAN, L. A control method for battery energy storage system based on mmc. In: *2015 IEEE 2nd International Future Energy Electronics Conference (IFEEC)*. [S.l.: s.n.], 2015. p. 1–6. 15

CHOI, J.; HAN, B.; KIM, H. New scheme of phase-shifted carrier pwm for modular multilevel converter with redundancy submodules. *IEEE Trans. on Power Delivery*, v. 31, n. 1, p. 407–409, Feb 2016. ISSN 0885-8977. 21

DEKKA, A. et al. Evolution of topologies, modeling, control schemes, and applications of modular multilevel converters. *IEEE Journal of Emerging and Selected Topics in Power Electronics*, v. 5, n. 4, p. 1631–1656, Dec 2017. ISSN 2168-6777. 16

DU, S.; LIU, J. A study on dc voltage control for chopper-cell-based modular multilevel converters in d-statcom application. *IEEE Transactions on Power Delivery*, v. 28, n. 4, p. 2030–2038, Oct 2013. ISSN 0885-8977. 15

FARIAS, J. V. M. et al. Design and lifetime analysis of a dscc-mmc statcom. In: *2017 Brazilian Power Electronics Conference (COBEP)*. [S.l.: s.n.], 2017. p. 1–6. 26

FARIAS, J. V. M. et al. On the redundancy strategies of modular multilevel converters. *IEEE Trans. on Power Delivery*, v. 33, n. 2, p. 851–860, April 2018. ISSN 0885-8977. 16, 18, 21, 22

GEMMELL, B. et al. Prospects of multilevel vsc technologies for power transmission. In: *IEEE/PES Transmission and Distrib. Conf. and Exposition*. [S.l.: s.n.], 2008. p. 1–16. ISSN 2160-8555. 18

HAGIWARA, M.; AKAGI, H. Control and experiment of pulsewidth-modulated modular multilevel converters. *IEEE Trans. on Power Electronics*, v. 24, n. 7, p. 1737–1746, July 2009. ISSN 0885-8993. 15, 20

HAGIWARA, M.; AKAGI, H. Experiment and simulation of a modular push–pull pwm converter for a battery energy storage system. *IEEE Transactions on Industry Applications*, v. 50, n. 2, p. 1131–1140, March 2014. ISSN 0093-9994. 15

HAGIWARA, M.; HASEGAWA, I.; AKAGI, H. Start-up and low-speed operation of an electric motor driven by a modular multilevel cascade inverter. *IEEE Trans. on Industry Applications*, v. 49, n. 4, p. 1556–1565, July 2013. ISSN 0093-9994. 15, 16, 18, 19, 20

HAGIWARA, M.; NISHIMURA, K.; AKAGI, H. A medium-voltage motor drive with a modular multilevel pwm inverter. *IEEE Trans. on Power Electronics*, v. 25, n. 7, p. 1786–1799, July 2010. ISSN 0885-8993. 16, 19, 20

HAMMOND, P. W. A new approach to enhance power quality for medium voltage ac drives. *IEEE Trans. on Industry Applications*, v. 33, n. 1, p. 202–208, Jan 1997. ISSN 0093-9994. 15

HARNEFORS, L. et al. Dynamic analysis of modular multilevel converters. *IEEE Trans. on Industrial Electronics*, v. 60, n. 7, p. 2526–2537, July 2013. ISSN 0278-0046. 18

JUNG, J.; LEE, H.; SUL, S. Control strategy for improved dynamic performance of variable-speed drives with modular multilevel converter. *IEEE Journal of Emerging and Selected Topics in Power Electronics*, v. 3, n. 2, p. 371–380, June 2015. ISSN 2168-6777. 15

KAWAMURA, W. et al. A low-speed, high-torque motor drive using a modular multilevel cascade converter based on triple-star bridge cells (mmcc-tsbc). *IEEE Trans. on Industry Applications*, v. 51, n. 5, p. 3965–3974, Sept 2015. ISSN 0093-9994. 15

KONSTANTINOU, G. S.; CIOBOTARU, M.; AGELIDIS, V. G. Effect of redundant sub-module utilization on modular multilevel converters. In: *IEEE International Conf. on Ind. Technology*. [S.l.: s.n.], 2012. p. 815–820. 21, 22

KOURO, S. et al. Powering the future of industry: High-power adjustable speed drive topologies. *IEEE Industry Applications Magazine*, v. 18, n. 4, p. 26–39, July 2012. ISSN 1077-2618. 15

KUMAR, Y. S.; PODDAR, G. Control of medium-voltage ac motor drive for wide speed range using modular multilevel converter. *IEEE Trans. on Ind. Electronics*, v. 64, n. 4, p. 2742–2749, April 2017. ISSN 0278-0046. 16

KUMAR, Y. S.; PODDAR, G. Medium-voltage vector control induction motor drive at zero frequency using modular multilevel converter. *IEEE Trans. on Industrial Electronics*, v. 65, n. 1, p. 125–132, Jan 2018. ISSN 0278-0046. 15, 16

LI, B. et al. Seamless transition control for modular multilevel converters when inserting a cold-reserve redundant submodule. *IEEE Trans. on Power Electronics*, v. 30, n. 8, p. 4052–4057, Aug 2015. ISSN 0885-8993. 21

LI, B. et al. A hybrid modular multilevel converter for medium-voltage variable-speed motor drives. *IEEE Trans. on Power Electronics*, v. 32, n. 6, p. 4619–4630, June 2017. ISSN 0885-8993. 16

LIU, G. et al. Optimized control strategy based on dynamic redundancy for the modular multilevel converter. *IEEE Trans. on Power Electronics*, v. 30, n. 1, p. 339–348, Jan 2015. ISSN 0885-8993. 16

MEYNARD, T. A. et al. Multicell converters: basic concepts and industry applications. *IEEE Trans. on Industrial Electronics*, v. 49, n. 5, p. 955–964, Oct 2002. ISSN 0278-0046. 20

NOVOTNY, D. W.; LIPO, T. *Vector Control and Dynamics of AC Drives*. [S.l.]: Clarendon Press, 1996. ISBN 9780198564393. 20, 24

PEDRA, J.; CORCOLES, F. Estimation of induction motor double-cage model parameters from manufacturer data. *IEEE Transactions on Energy Conversion*, v. 19, n. 2, p. 310–317, June 2004. ISSN 0885-8969. 27

PENG, F. Z. et al. A multilevel voltage-source inverter with separate dc sources for static var generation. In: *IAS '95. Conference Record of the 1995 IEEE Industry Applications Conference Thirtieth IAS Annual Meeting*. [S.l.: s.n.], 1995. v. 3, p. 2541–2548 vol.3. ISSN 0197-2618. 15

PEREIRA, H. A.; CUPERTINO, A. F.; JUNIOR, S. I. S. *Basic Concepts of Modular Multilevel Converters and Applications in Medium and High Voltage Fields*. [S.l.]: COBEP 2017 Tutorials, 2017. 01-91 p. 15

SAAD, H. et al. Mmc capacitor voltage decoupling and balancing controls. *IEEE Trans. on Power Delivery*, v. 30, n. 2, p. 704–712, April 2015. ISSN 0885-8977. 21

SAHOO, S. K.; BHATTACHARYA, T. Phase-shifted carrier-based synchronized sinusoidal pwm techniques for a cascaded h-bridge multilevel inverter. *IEEE Trans. on Power Electronics*, v. 33, n. 1, p. 513–524, Jan 2018. ISSN 0885-8993. 20

SIEMENS. *Sinamics SM 120 CM*. [S.l.], 2018. Disponível em: <https://www.industry.siemens.com/drives/global/en/converter/mv-drives/Pages/sinamics-sm120-cm.aspx>. 9, 16

SON, G. T. et al. Design and control of a modular multilevel hvdc converter with redundant power modules for noninterruptible energy transfer. *IEEE Trans. on Power Delivery*, v. 27, n. 3, p. 1611–1619, July 2012. ISSN 0885-8977. 16, 21

SONG, Y.; WANG, B. Survey on reliability of power electronic systems. *IEEE Trans. on Power Electronics*, v. 28, n. 1, p. 591–604, Jan 2013. ISSN 0885-8993. 16

TU, Q.; XU, Z. Power losses evaluation for modular multilevel converter with junction temperature feedback. In: *IEEE Power and Energy Society General Meeting*. [S.l.: s.n.], 2011. p. 1–7. ISSN 1932-5517. 26

WANG, B. et al. Reliability model of mmc considering periodic preventive maintenance. *IEEE Trans. on Power Delivery*, v. 32, n. 3, p. 1535–1544, June 2017. ISSN 0885-8977. 16

WEG. *HGF*. [S.l.], 2018. Disponível em: <https://static.weg.net/medias/downloadcenter/h8e/h68/WEG-hgf-motor-trifasico-de-inducao-50029374-brochure-portuguese-web.pdf>. 27

WEG. *HGF - Linha não acendível*. [S.l.], 2018. Disponível em: <https://www.weg.net/catalog/weg/BR/pt/Motores-El%C3%A9tricos/Trif%C3%A1sico---Alta-Tens%C3%A3o/Atmosferas-Explosivas/HGF-%28N%C3%A3o-Acend%C3%ADvel%29/HGF-N%C3%A3o-Acend%C3%ADvel/p/MKT_WMO_BR_HGF_NAO_ACENDIVEL_MEDIA_TENSAO>. 8, 27

XU, C. et al. Unbalanced pcc voltage regulation with positive- and negative-sequence compensation tactics for mmc-dstatcom. *IET Power Electronics*, v. 9, n. 15, p. 2846–2858, 2016. ISSN 1755-4535. 19

ZHANG, L. et al. Modeling, control, and protection of modular multilevel converter-based multi-terminal hvdc systems: A review. *CSEE Journal of Power and Energy Systems*, v. 3, n. 4, p. 340–352, Dec 2017. ISSN 2096-0042. 15